Optical-field-dependent electron-electron scattering effects and gain generation in the intersubband transitions of n-doped quantum wells

1998 J. Phys.: Condens. Matter 10 2489

(http://iopscience.iop.org/0953-8984/10/11/013)

J. Phys.: Condens. Matter **10** (1998) 2489–2503. Printed in the UK PII: S0953-8984(98)86256-5

Optical-field-dependent electron–electron scattering effects and gain generation in the intersubband transitions of n-doped quantum wells

S M Sadeghi, S R Leffler, J Meyer and E Mueller†

The University of British Columbia, Department of Physics and Astronomy, 6224 Agricultural Road, Vancouver, BC, V6T 1Z1, Canada

Received 24 July 1997, in final form 25 November 1997

Abstract. We study the effect of electron–electron scattering on the polarization dephasing rates of infrared-coupled intersubband transitions in n-doped quantum wells. By numerical solution of the Boltzmann and optical Bloch equations we show how these rates depend on the properties of the infrared field and the doped quantum well. We also determine the electron distributions in each subband for various field intensities and detunings. We show that when the system is probed by a weak infrared field, a tunable Raman-type gain spectrum can be generated under certain conditions.

1. Introduction

Intersubband transitions in n-doped quantum well (QW) structures have attracted a great deal of attention in recent years. They have important practical applications such as semiconductor lasers and infrared (IR) detectors [1, 2] and can be used to study two-dimensional electron gas systems, intersubband scattering rates of electrons, nonlinear processes in QWs, etc [3–9]. In these studies an IR field polarized along the growth direction of a QW strongly couples the ground subband to a higher one. Nearly all of these studies assume that the energy relaxation rates of electrons in the conduction subbands and the dephasing rates of polarization associated with the intersubband transitions are independent of the electron wavevector and are mainly caused by electron–phonon scattering [6–11]. As a result, the relaxation time approximation (RTA) has been applied extensively to describe the damping of the diagonal elements of the density matrix even when the IR intensity is not small. Similar assumptions have been made in the discussion of optical intersubband transitions in p-type structures [12].

We show in this paper that considering the electron–electron scattering process calls into question the validity of these assumptions. Various effects of electron–electron scattering have been studied in recent years, including renormalization of the intersubband transition energy, and excitonic effects (vortex correction of the polarization) [10, 11, 13]. The effects on the damping rates of polarization and of electron energy remain untackled, however. To our knowledge, all previous studies have modelled these rates phenomenologically using constant parameters [6–13]. Intersubband transitions involving the ground subband are

† Present address: Department of Physics, University of Illinois at Urbana-Champaign, 1110 W Green Street, Urbana, IL 61801, USA.

0953-8984/98/112489+15$19.50

strongly affected by the electron–electron scattering process, though, which implies that the actual rates depend on the electron wavevector (k), distribution function and density. Even when the infrared field only weakly perturbs the ground subband distribution function so that the RTA is valid (the weak-field regime), the strong k dependence implies that one cannot consider the damping rates to be constant for all values of k. This means that the traditional assumption of homogeneous transition rates for all k is invalid even for weak driving fields.

When the IR intensity is not weak, three major issues are raised which to our knowledge also remain unexplored. First, the IR field generates non-Fermi steady-state electron distributions in both of the coupled subbands. Second, saturation effects can be seen once the higher subband is significantly occupied. This case has been studied in the past by employing the RTA and ignoring electron–electron scattering [6–9]. A consistent treatment requires solving the Boltzmann equation in the presence of the IR field, instead. Third, one can use an additional weak IR field to induce quantum interference and gain processes in a simple two-subband QW system. This concept is very appealing for generation of far-infrared lasers in QWs.

The goal of this paper is to address these issues by considering a rigorous treatment of intersubband transitions in n-doped QWs including the mutual effects of the screened electron–electron scattering process and the transitions on each other. We show that the damping rates of electrons and polarization not only depend on the temperature, the electron distribution function, the density, the effective mass, and the QW parameters, but also on the IR intensity and frequency. In the strong-field regime we also discuss the quantum interference and gain processes when the strongly driven n-doped QW is probed by a weak field with the same polarization as the driving field. Our investigation shows that the linear response of the system to the weak field can have a Mollow spectrum similar to that observed in atomic systems [14]. This includes generation of gain with hidden inversion (Raman gain), and gain caused by stimulated Rayleigh scattering. We show that the Raman gain in this system is tunable over a range of frequencies comparable to that of the intersubband transition, just by changing the intensity of the driving field. Also, in the strong-field regime we calculate the absorption coefficient using a non-perturbative approach. Our results show significant differences from those obtained using perturbative RTA-based approaches [7, 8].

In section 2 of this paper we present our formalism which deals with linear and non-linear intersubband transitions in n-doped QWs. In section 3 we study the polarization dephasing rates caused by electron–electron scattering in the weak-field regime. The dynamic evolution of the electron distribution functions and polarization dephasing rates in the presence of a strong IR field is studied in section 4 for various field intensities and frequencies. In section 5 we revisit the saturation effects in the absorption coefficient of this system. In section 6 we discuss the linear response of the system to a probe field. Sections 7 and 8 contain discussion and concluding remarks.

2. Formalism

We are interested in the interaction of an IR field with an n-doped QW. This field is considered to be resonant or nearly resonant with the transition between the first and the second conduction subbands (1–2) and quite off-resonant with all other transitions. We assume that in the absence of the IR field only the ground subband is occupied, with a Fermi–Dirac distribution. In the rotating-wave and dipole approximations the coupling of this electronic system with the IR field, $E(t) = E\mathrm{e}^{-\mathrm{i}\omega t}$, polarized along the QW growth

direction, z, can be described by the Hamiltonian

$$H_{\rm int} = \overline{h} \sum_{\boldsymbol{k}} \{\mu_{12} E(t) c^{\dagger}_{1,\boldsymbol{k}} c_{2,\boldsymbol{k}} + \mu^{*}_{12} E^{*}(t) c^{\dagger}_{2,\boldsymbol{k}} c_{1,\boldsymbol{k}}\}. \tag{1}$$

Here μ_{12} is the electric dipole moment for the transition between the first and second conduction subbands along the z direction, which is assumed to be $\boldsymbol{k}$-independent. $c_{i,\boldsymbol{k}}$ and $c^{\dagger}_{i,\boldsymbol{k}}$ are respectively the annihilation and creation operators of an electron in $|i, \boldsymbol{k}\rangle$ (the state of an electron with wavevector $\boldsymbol{k}$ and subband index i) with energy $E^{c}(i, k)$.

The density matrix elements of this system in the presence of the IR field can be obtained from

$$\frac{\partial \rho}{\partial t} = -\frac{\mathrm{i}}{\overline{h}}[H_0 + H_{\rm int}, \rho] + \left.\frac{\partial \rho}{\partial t}\right|_{\rm relax}. \tag{2}$$

Here H_0 is the Hamiltonian of the system in the absence of the infrared field, and $(\partial\rho/\partial t)|_{\rm relax}$ refers to the relaxation terms of the density matrix. In general this term has two components:

$$\left.\frac{\partial \rho}{\partial t}\right|_{\rm relax} = \left.\frac{\partial \rho}{\partial t}\right|_{\rm e-e} + \left.\frac{\partial \rho}{\partial t}\right|_{\rm e-p}. \tag{3}$$

The first term on the right-hand side represents the relaxation process caused by electron–electron scattering. For diagonal elements of the density matrix it is given by the Boltzmann equation:

$$\left.\frac{\mathrm{d}\rho^{\boldsymbol{k}}_{ii}}{\mathrm{d}t}\right|_{\rm e-e} = \Gamma^{\rm in}_{i}(\boldsymbol{k}, \rho^{\boldsymbol{k}}_{ii})(1 - \rho^{\boldsymbol{k}}_{ii}) - \Gamma^{\rm out}_{i}(\boldsymbol{k}, \rho^{\boldsymbol{k}}_{ii})\rho^{\boldsymbol{k}}_{ii}. \tag{4}$$

Here $\Gamma^{\rm in}_{i}(\boldsymbol{k}, \rho^{\boldsymbol{k}}_{ii})$ and $\Gamma^{\rm out}_{i}(\boldsymbol{k}, \rho^{\boldsymbol{k}}_{ii})$ are the scattering in and out rates at $|i, \boldsymbol{k}\rangle$ due to the electron–electron scattering process. They are given by

$$\begin{aligned}\Gamma^{\rm in}_{i}(\boldsymbol{k}, \rho_{ii}) = {} & \frac{4\pi}{\overline{h}} \sum_{\boldsymbol{p},\boldsymbol{q}} \rho^{\boldsymbol{p}}_{ii} \rho^{\boldsymbol{k}-\boldsymbol{q}}_{ii} (1 - \rho^{\boldsymbol{p}-\boldsymbol{q}}_{ii}) |V_i(q, \overline{h}\omega')|^2 \\ & \times \delta(E^{c}(i, \boldsymbol{k}) + E^{c}(i, \boldsymbol{p} - \boldsymbol{q}) - E^{c}(i, \boldsymbol{k} - \boldsymbol{q}) - E^{c}(i, \boldsymbol{p}))\end{aligned} \tag{5}$$

and

$$\begin{aligned}\Gamma^{\rm out}_{i}(\boldsymbol{k}, \rho_{ii}) = {} & \frac{4\pi}{\overline{h}} \sum_{\boldsymbol{p},\boldsymbol{q}} (1 - \rho^{\boldsymbol{p}}_{ii}) \rho^{\boldsymbol{p}-\boldsymbol{q}}_{ii} (1 - \rho^{\boldsymbol{k}-\boldsymbol{q}}_{ii}) |V_i(q, \overline{h}\omega')|^2 \\ & \times \delta(E^{c}(i, \boldsymbol{k}) + E^{c}(i, \boldsymbol{p} - \boldsymbol{q}) - E^{c}(i, \boldsymbol{k} - \boldsymbol{q}) - E^{c}(i, \boldsymbol{p})).\end{aligned} \tag{6}$$

Here $V_i(q, \overline{h}\omega')$ is the screened electron–electron interaction given by

$$V_i(q, \overline{h}\omega') = \frac{v_q F_i(q)}{\epsilon_i(q, \overline{h}\omega')} \tag{7}$$

where $v_q = 2\pi e^2/(Sq\epsilon_b)$, e is the electric charge, S the area of the QW and ϵ_b is the bulk dielectric constant which is assumed to be the same in the QW and in the barrier. Also $\overline{h}\omega' = E^{c}(i, \boldsymbol{k} - \boldsymbol{q}) - E^{c}(i, \boldsymbol{k})$, and the form factor $F_i(q)$ is given by

$$F_i(q) = \iint |\phi_i(z)\phi_i(z')|^2 \, \mathrm{e}^{-q|z-z'|} \, \mathrm{d}z \, \mathrm{d}z'. \tag{8}$$

Here $\phi_i(z)$ is the confinement wave function for the ith conduction subband. The screened dynamic dielectric function due to the quasi-two-dimensional electron gas is given by

$$\epsilon_i(q, \omega) = 1 + v_q F_i(q) \chi_i(q, \omega) \tag{9}$$

where

$$\chi_i(q,\omega) = 2\sum_{\boldsymbol{p},\delta\to\boldsymbol{0}} \frac{\rho_{ii}^{\boldsymbol{p}} - \rho_{ii}^{\boldsymbol{p}-\boldsymbol{q}}}{E^c(i,\boldsymbol{p}-\boldsymbol{q}) - E^c(i,\boldsymbol{p}) + \hbar\omega - \mathrm{i}\delta}. \tag{10}$$

The contribution of the electron–electron scattering process to the dephasing rates of the system is determined according to

$$\left.\frac{\partial\rho_{ij}^{\boldsymbol{k}}}{\partial t}\right|_{\mathrm{e-e}} = -\gamma_{ij}^{\mathrm{e-e}}(k)\rho_{ij}^{\boldsymbol{k}} + \left.\frac{\partial\rho_{ij}^{\boldsymbol{k}}}{\partial t}\right|_{\mathrm{nd}}^{\mathrm{e-e}} \qquad i \neq j \tag{11}$$

where $\gamma_{ij}^{\mathrm{e-e}}(k)$, the diagonal contribution to the dephasing rate, is given by

$$\gamma_{ij}^{\mathrm{e-e}}(k) = -\mathrm{Im}\,(\Sigma_i^{\mathrm{e-e}}(k) + \Sigma_j^{\mathrm{e-e}}(k)). \tag{12}$$

Here $\Sigma_i^{\mathrm{e-e}}$ is the retarded self-energy which is related to Γ_i^{out} and Γ_i^{in} by

$$\mathrm{Im}\,\Sigma_i^{\mathrm{e-e}}(k) = -\tfrac{1}{2}(\Gamma_i^{\mathrm{in}}(k) + \Gamma_i^{\mathrm{out}}(k)). \tag{13}$$

The second term of (11) refers to the non-diagonal contribution of the electron–electron scattering process to the polarization dephasing rate. This term describes the rate of polarization transfer between the state $\boldsymbol{k}$ and other states, due to the scattering process. It has been shown that this term plays a significant role, in that it partially cancels the diagonal contribution, affecting the gain lineshape in inverted semiconductors [15, 16]. In the limit of high electron density, however, one can neglect this term due to strong screening, as shown in [15]. Therefore we consider only the dephasing given by (12) and (13) [17]. Also note that in the above discussion we have ignored any intersubband transitions caused by electron–electron scattering. This process can be significant when the energy spacing between the subbands is small [18].

Returning to (3), the second term represents the electron–phonon scattering process' contribution to the damping of the electronic system. This depends on the kinetic energy of the electrons and which subband they are in. For the ground subband, if the Fermi energy is less than the energy of longitudinal–optical phonons (LO phonons) the only such process is electron–acoustic phonon scattering. This process is weak and diffusive [19]. The upper subband is assumed to be separated from the ground subband by an energy greater than the LO phonon energy. Since the electron envelope functions in this subband are asymmetric and much less localized than those in the ground state, the dominant energy relaxation mechanism is intersubband transition via emission of LO phonons. This means that the damping rates due to electron–electron scattering are always either fast (in $|1,\boldsymbol{k}\rangle$) or slow (in $|2,\boldsymbol{k}\rangle$) relative to the rates due to electron–phonon scattering. We therefore represent the latter phenomenologically. This is consistent with the fact that electron–phonon scattering is nearly independent of k for electrons with kinetic energies less than the LO phonon energy [19]. The electron–phonon scattering processes are thus represented in our model by

$$\left.\frac{\mathrm{d}\rho_{11}^{\boldsymbol{k}}}{\mathrm{d}t}\right|_{\mathrm{e-p}} = \left.\frac{\mathrm{d}\rho_{11}^{\boldsymbol{k}}}{\mathrm{d}t}\right|_{\mathrm{diff}} \tag{14}$$

and

$$\left.\frac{\mathrm{d}\rho_{22}^{\boldsymbol{k}}}{\mathrm{d}t}\right|_{\mathrm{e-p}} = -\Gamma_2^p\rho_{22}^{\boldsymbol{k}}. \tag{15}$$

Here Γ_2^p is the intersubband transition rate of an electron in the second subband due to emission of LO phonons. (14) explicitly refers to the diffusive nature of electron energy relaxation in the first subband. For the off-diagonal terms we have

$$\left.\frac{\mathrm{d}\rho_{ij}^{\boldsymbol{k}}}{\mathrm{d}t}\right|_{\mathrm{e-p}} = -\gamma_{ij}^{p}\rho_{ij}^{\boldsymbol{k}} \tag{16}$$

where γ_{ij}^{p} is the dephasing rate caused by the electron–phonon scattering process. This is given by

$$\gamma_{12}^{p} = \tfrac{1}{2}(\Gamma_2^p + \Gamma_1^p) \tag{17}$$

where Γ_1^p is the electron–acoustic phonon scattering rate.

From the above, one can derive the equations of motion for the density matrix elements:

$$\frac{\mathrm{d}\rho_{11}^{\boldsymbol{k}}}{\mathrm{d}t} = -\mathrm{i}\Omega_{12}(\rho_{21}^{\boldsymbol{k}} - \rho_{12}^{\boldsymbol{k}}) + \left.\frac{\mathrm{d}\rho_{11}^{\boldsymbol{k}}}{\mathrm{d}t}\right|_{\mathrm{e-e}} + \left.\frac{\mathrm{d}\rho_{11}^{\boldsymbol{k}}}{\mathrm{d}t}\right|_{\mathrm{diff}} + P_{kk'} \tag{18}$$

$$\frac{\mathrm{d}\rho_{22}^{\boldsymbol{k}}}{\mathrm{d}t} = \mathrm{i}\Omega_{12}(\rho_{21}^{\boldsymbol{k}} - \rho_{12}^{\boldsymbol{k}}) - \Gamma_2^p\rho_{22}^{\boldsymbol{k}} \tag{19}$$

and

$$\frac{\mathrm{d}\rho_{21}^{\boldsymbol{k}}}{\mathrm{d}t} = -\mathrm{i}[\Delta_k - \mathrm{i}\gamma_{12}^{\mathrm{e-e}}(k) - \mathrm{i}\gamma_{12}^{p}]\rho_{21}^{\boldsymbol{k}} - \mathrm{i}\Omega_{12}(\rho_{11}^{\boldsymbol{k}} - \rho_{22}^{\boldsymbol{k}}). \tag{20}$$

Here $\Omega_{12} = -\mu_{12}E/\overline{h}$ is the Rabi frequency of the IR field. $P_{kk'}$ is the population rate of $|1, \boldsymbol{k}\rangle$ due to relaxation of electrons out of states in the second conduction subband with wavevector k'. This term includes both the intersubband transition and the subsequent cascade in the ground subband due to LO phonon decay. Since here the electron probability is calculated in each subband, in contrast to previous studies which only calculated $\rho_{22} - \rho_{11}$ [7, 8], it is crucial to consider such a term. In general (18) can have a complicated form since $P_{kk'}$ couples states with different wavevectors k. However, in the case where the energy spacing of the subbands is nearly equal to an integer number of LO phonon energies ($E^c(2,k) - E^c(1,k) = n\overline{h}\Omega_{\mathrm{LO}}$) the problem becomes tractable. In this case we can impose the condition that

$$\rho_{11}^{k} + \rho_{22}^{k} \sim \rho_{11}^{0k}. \tag{21}$$

Here ρ_{11}^{0k} is the Fermi–Dirac distribution of the ground subband in the absence of any IR field. This yields $P_{kk'} \sim \Gamma_2^p\rho_{22}^{k}\delta_{kk'}$. As will be shown in section 4, the requirement that $E^c(2,k) - E^c(1,k) = n\overline{h}\Omega_{\mathrm{LO}}$ can be relaxed in the case of high field intensity.

Regarding (18)–(20), one should note that the internal field effect terms which renormalize the Rabi frequency have been neglected. This is because, as discussed in [20], for high excitation screening plays a major role and reduces the effect of these terms.

Note also that since the electron density is considered to be high, the depolarization effect can renormalize the detuning

$$\Delta_k = \frac{E^c(2,k)}{\overline{h}} - \frac{E^c(1,k)}{\overline{h}} - \omega \tag{22}$$

which appears in (20) [21]. Additionally, $E^c(i,k)$ can be affected by the self-energies [11–13, 22] and by the band bending effect. The latter depends on how the QW is doped, and is expected to have an insignificant effect for uniformly doped structures [23].

To study the linear response of the system discussed above, we consider an optical probe field with the same polarization as the strong field. This field does not perturb the system significantly. This case is similar to that studied by Mollow in atomic systems [14], but

is complicated by the momentum dependence of intersubband transitions in n-doped QWs. To find the linear response of the system to the probe field we use linear response theory and the quantum regression theorem. The absorption spectrum of the weak probe field is found to have the form

$$A(\omega_p) = \mathrm{Re} \sum_{\boldsymbol{k}} \rho_{11}^{k} \langle [p_{\boldsymbol{k}}^{+}(t'), \hat{p}_{\boldsymbol{k}}^{-}(z, t')] \rangle|_{z=\mathrm{i}\omega_p}. \tag{23}$$

Here ω_p is the probe frequency. $p_{\boldsymbol{k}}^{-}$ and $p_{\boldsymbol{k}}^{+}$ are the negative and positive frequency components of the system polarization at a specific $\boldsymbol{k}$, given by

$$p_{\boldsymbol{k}}^{+}(t) = \mu_{12} c_{1,\boldsymbol{k}}^{\dagger}(t) c_{2,\boldsymbol{k}}(t) \tag{24}$$

and

$$p_{\boldsymbol{k}}^{-}(t) = [p_{\boldsymbol{k}}^{+}(t)]^{*}. \tag{25}$$

$\hat{p}_{\boldsymbol{k}}^{-}(z, t')$ is the Laplace transform of $p_{\boldsymbol{k}}^{-}(t = \tau + t')$ with respect to $\tau = t - t'$ with $\tau > 0$. For steady state conditions ($t, t' \to \infty$),

$$\langle [\hat{p}_{\boldsymbol{k}}^{+}(\infty), \hat{p}_{\boldsymbol{k}}^{-}(z)] \rangle = \mu_{01}^{2} \{ \rho_{21}^{k}(\infty) [R_{32}^{k}(z) - R_{31}^{k}(z)] - R_{33}^{k} [\rho_{11}^{k}(\infty) - \rho_{22}^{k}(\infty)] \}. \tag{26}$$

Here $R_{ij}^{k}(z)$ are the elements of the matrix

$$\mathbf{R}^{k}(z) = \begin{pmatrix} z + \Gamma_2^p & 0 & -\mathrm{i}\Omega & \mathrm{i}\Omega \\ 0 & z + \Gamma_2^p & \mathrm{i}\Omega & -\mathrm{i}\Omega \\ \mathrm{i}\Omega & -\mathrm{i}\Omega & z - \mathrm{i}[\Delta_k + \mathrm{i}(\gamma_{12}^{\mathrm{e-e}}(k) + \gamma_{12}^{p})] & 0 \\ -\mathrm{i}\Omega & \mathrm{i}\Omega & 0 & z + \mathrm{i}[\Delta_k - \mathrm{i}(\gamma_{12}^{\mathrm{e-e}}(k) + \gamma_{12}^{p})] \end{pmatrix}^{-1}.$$

The absorption coefficient of the intersubband transition is given by

$$\alpha(\omega) = \omega \sqrt{\frac{\mu}{\epsilon_R}} \mathrm{Im}\,[\epsilon_0 \chi'(\omega)]. \tag{27}$$

Here μ and ϵ_R are the permeability and the real part of the permittivity, respectively. $\chi'(\omega)$ is the susceptibility of the system for the particular transition, given by

$$\chi'(\omega) = \frac{1}{\pi \epsilon L_{\mathrm{eff}}} \int_0^{k_{\max}} k\,\mathrm{d}k \frac{|\mu_{12}|^2 (\rho_{11}^{k} - \rho_{22}^{k})}{\overline{h}[\Delta_k - \mathrm{i}(\gamma_{12}^{\mathrm{e-e}}(k) + \gamma_{12}^{p})]} \tag{28}$$

where L_{eff} is the effective length over which the interaction occurs, taken to be the width of the QW. One difference between (28) and the analogous equation used in the previous investigations [7–11] is the addition of $\gamma_{12}^{\mathrm{e-e}}$ in the denominator. Another significant difference between our approach for calculation of $\alpha(\omega)$ and those previously reported is that we calculate $\alpha(\omega)$ accurately. In the past, perturbative methods have usually been used to find the response of QWs in terms of various orders of the susceptibility [7–9]. As we find in section 5, the results of our approach are very different from those of the perturbative methods.

3. Electron–electron scattering effects on the intersubband polarization dephasing rates in the weak-field regime

In this section we study how the electron–electron scattering process contributes to the polarization dephasing rate $\gamma_{12}^{\mathrm{e-e}}(k)$ in the weak-field limit. In this limit, depletion of the ground subband population by the IR field is ignored, and (12) and (13) reduce to $\gamma_{12}^{\mathrm{e-e}}(k) = \frac{1}{2}(\Gamma_1^{\mathrm{out}} + \Gamma_1^{\mathrm{in}})$, evaluated using the zero-field population. Here $(\Gamma_1^{\mathrm{out}} + \Gamma_1^{\mathrm{in}})$ is the damping rate of quasi-holes (QHs) or kinetic holes, generated by transitions out of the

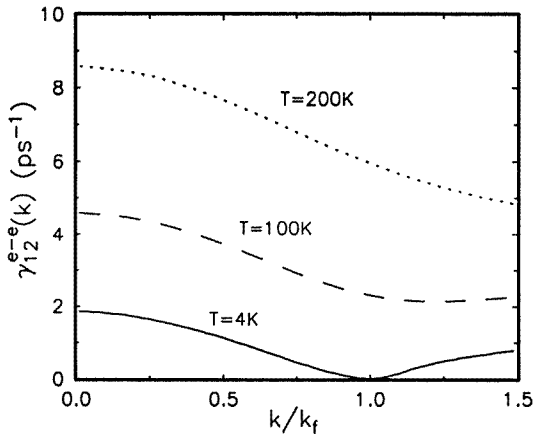

Figure 1. Polarization dephasing rates caused by electron–electron scattering for various temperatures for $Al_{0.3}Ga_{0.7}As$ with 6.5 nm well width. Density of electrons is 7×10^{11} cm^{-2}.

ground subband. These rates have been studied by Binder *et al* [17] and Lyo [24]. Binder's analysis was applicable only to QHs generated by interband transitions in inverted bulk semiconductors. Lyo's study considered QW structures, but did not use realistic structures for temperatures above 0 K. Lyo's work also gave little insight into how the damping rate varies with wavevector at elevated temperatures. In this section we present the results of numerical calculations of the QH damping rate for a realistic QW structure at temperatures above 0 K.

We first consider an n-doped $GaAs/Al_xGa_{1-x}As$ QW with 6.5 nm well width and $x = 0.3$. The effective mass of the electrons is taken as $0.07m_0$ (m_0 is the free electron mass), and the electron density is 7×10^{11} cm^{-2} ($\varepsilon_f = 24$ meV at 0 K). In figure 1 we show $\gamma_{12}^{e-e}(k)$ for various temperatures. For $T = 4$ K, $\gamma_{12}^{e-e}(k)$ decreases from a maximum value at $k = 0$ to ~ 0 at $k = k_f = 0.210$ nm^{-1} and then increases for $k > k_f$. This feature, which has been predicted by Binder for bulk semiconductors, becomes less significant at higher temperatures. At 100 and 200 K (dashed and dotted lines) $\gamma_{12}^{e-e}(k)$ is significantly higher for all k. For $T = 0$ K (not shown) the damping rate is very close to that shown for $T = 4$ K, for $k < k_f$. Our model is the same as that used by Lyo at 0 K [24], and gives identical results when applied to the structures Lyo considered. For higher temperatures, however, Lyo used a different model which produces results that disagree with those of the former model by up to a factor of two.

Next we examine how $\gamma_{12}^{e-e}(k)$ changes with conduction band offset. We consider $\Delta E_c = 107$ meV and $\Delta E_c = 213$ meV, which correspond to $x = 0.15$ and $x = 0.3$ respectively, and $\Delta E_c = 10$ eV [11]. The last case is not realistic but is an approximation to the infinite-well model used by others [24]. The material structure is the same as that of figure 1 with the same electron density and well width. The temperature is 4 K. Figure 2 shows that, for states far from the Fermi edge, increasing the value of the offset causes an increase in $\gamma_{12}^{e-e}(k)$. This is because as the band offset increases, the electrons become more confined and the strength of their interaction with other electrons increases.

Figure 3 shows the effect of electron density on $\gamma_{12}^{e-e}(k)$ at 4 K, using the same structure as in figure 1. All of the densities are chosen such that the Fermi energy is less than the LO phonon energy ($n = 5 \times 10^{11}$ cm^{-2} with $\varepsilon_f = 17$ meV; $n = 2 \times 10^{11}$ cm^{-2} with $\varepsilon_f = 6.8$ meV). As the electron density decreases $\gamma_{12}^{e-e}(k)$ is significantly reduced over a

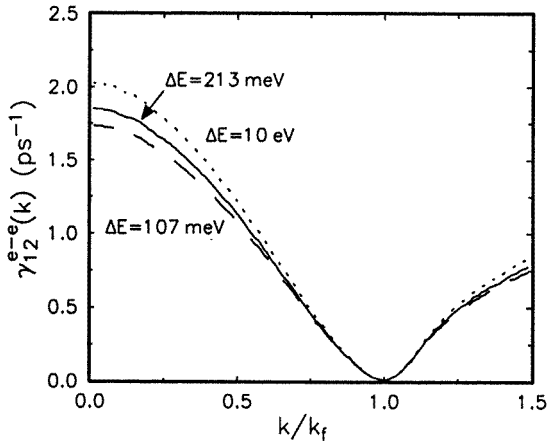

Figure 2. Polarization dephasing rates caused by electron–electron scattering for various conduction band offsets for $Al_xGa_{1-x}As$ at $T = 4$ K. All other specifications are the same as those of figure 1.

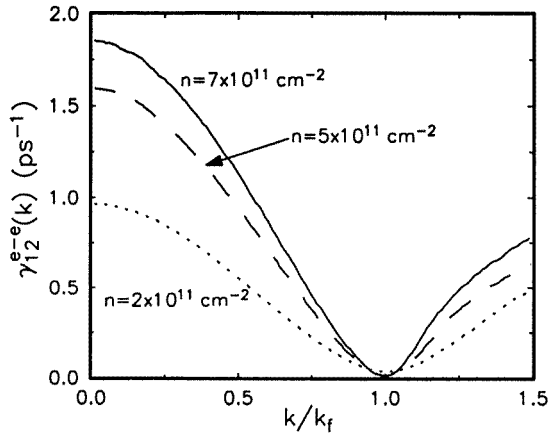

Figure 3. Polarization dephasing rates caused by electron–electron scattering for various electron densities for $Al_{0.3}Ga_{0.7}As$ with 6.5 nm well width at $T = 4$ K. All other specifications are the same as those of figure 1.

large range of k. In the vicinity of the Fermi energy, however, there is a slight increase in the dephasing rate.

4. Field-dependent electron–electron scattering effects in the intersubband transition of quantum wells

To study the electron–electron scattering effects in the intersubband transition of a QW under an intense IR field, one must simultaneously solve the Boltzmann equation and the optical Bloch equations (18)–(20). From (11)–(13), the scattering-out and in terms of (4) directly affect the dephasing rates of intersubband transitions. These rates therefore depend on the

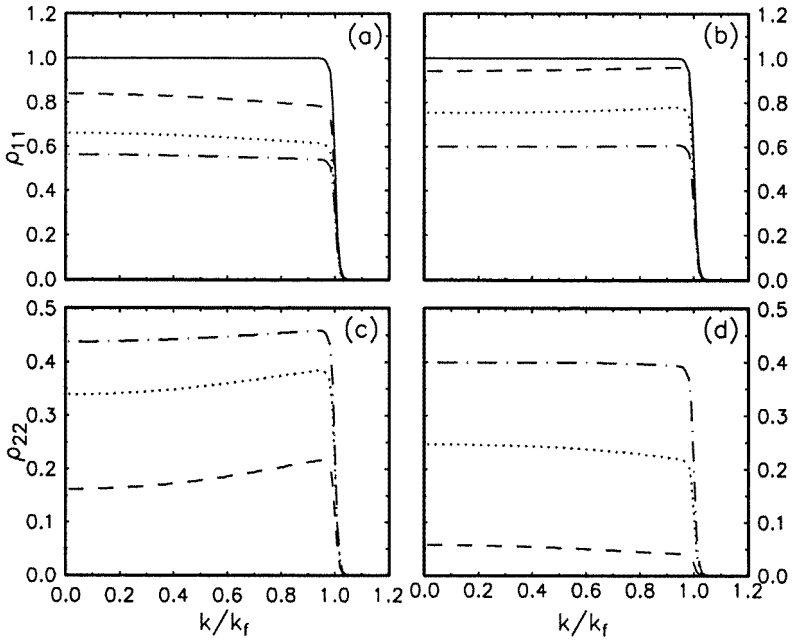

Figure 4. Electron distribution functions. The solid lines correspond to $\Omega_{12} = 0$ ps^{-1}, dashed lines to $\Omega_{12} = 2$ ps^{-1}, dotted line to $\Omega_{12} = 5$ ps^{-1} and dashed–dotted line to $\Omega_{12} = 10$ ps^{-1}. (a) and (b) show the distributions in the first subband for $\Delta = 0$ and $\Delta = 10$ ps^{-1}, respectively. (c) and (d) show the distributions in the second subband for the same respective cases.

IR frequency and intensity in addition to the electron density, QW structure, temperature etc. We assume that the IR field does not vary significantly on the scale of the system's characteristic dephasing time, allowing steady-state solution of (18)–(20). From (18) and (19),

$$\frac{\mathrm{d}\rho_{11}^{\boldsymbol{k}}}{\mathrm{d}t} + \frac{\mathrm{d}\rho_{22}^{\boldsymbol{k}}}{\mathrm{d}t} = \left.\frac{\mathrm{d}\rho_{11}^{\boldsymbol{k}}}{\mathrm{d}t}\right|_{\mathrm{e-e}} + \left.\frac{\mathrm{d}\rho_{11}^{\boldsymbol{k}}}{\mathrm{d}t}\right|_{\mathrm{diff}} + P_{kk'} - \Gamma_2^p \rho_{22}^{\boldsymbol{k}}. \tag{29}$$

In the steady state, the right-hand side of (29) is zero. From section 2, $P_{kk'} \sim \Gamma_2^p \rho_{22}^{\boldsymbol{k}}$, therefore

$$\left.\frac{\mathrm{d}\rho_{11}^{\boldsymbol{k}}}{\mathrm{d}t}\right|_{\mathrm{e-e}} + \left.\frac{\mathrm{d}\rho_{11}^{\boldsymbol{k}}}{\mathrm{d}t}\right|_{\mathrm{diff}} = 0. \tag{30}$$

Using this allows (18)–(20) to be solved, yielding the results shown in figure 4. We consider the same QW structure as used for figure 1 with $E^c(1,0) = 55$ meV and $E^c(2,0) = 199$ meV [25], and take $T = 4$ K, $\Gamma_2^p = 5$ ps^{-1}, and $\Gamma_1^p = 0.1$ ps^{-1}. Figure 4(a) shows the ground state electron distribution for $\Delta_k = 0$. In the presence of an IR field such that $\Omega_{12} = 2$ ps^{-1} (dashed lines), there is significant depletion of the initial Fermi distribution in $\rho_{11}^{\boldsymbol{k}}$. This depletion is non-uniform in k, however: states close to the Fermi energy are depleted more than others. As the field intensity is increased, $\rho_{11}^{\boldsymbol{k}}$ undergoes approximately linear depletion until $\Omega_{12} \simeq 5$ ps^{-1} (dotted line), where it begins to saturate. Further increase in Ω_{12} causes less change in ρ_{11}, as shown.

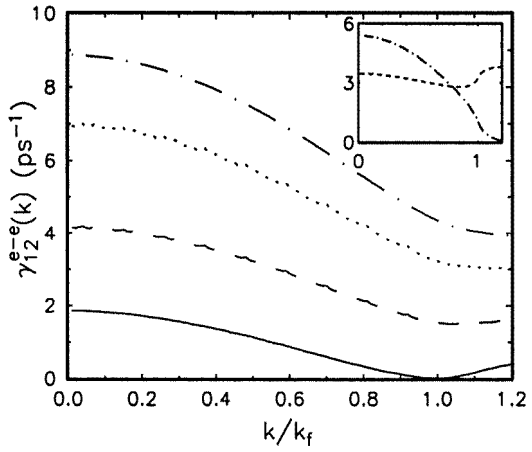

Figure 5. Polarization dephasing rates caused by electron–electron scattering corresponding to figure 4(a). Inset shows the contributions due to scattering in (dashed–dotted line) and scattering out (dashed line) for $\Omega = 10$ ps^{-1}.

Figure 4(c) shows the corresponding evolution of the electron distribution in the second subband. One can see that at low field intensity the electron distribution is not flat. As expected, increasing the infrared intensity causes the excited and ground states to become more equally populated. In the high-field limit where $\Omega_{12} \gg \gamma_{12}^{\mathrm{e-e}} + \gamma_{12}^{p}$ we have $\rho_{11}^{\boldsymbol{k}} = \rho_{22}^{\boldsymbol{k}} = 0.5$ for all $\boldsymbol{k}$.

The features seen in figure 4(a) and (c) are results of the electron–electron scattering process in the ground subband. To see this in more detail, we show in figure 5 the dephasing rates of polarization corresponding to the distribution functions shown in these figures. The solid line in this figure shows the rate corresponding to the undisturbed Fermi distribution ($\Omega_{12} = 0$). As the field intensity increases, the damping rates increase dramatically. For $\Omega_{12} = 2$ ps^{-1}, for example, the rate is increased by more than a factor of two. In other words, the IR field extensively broadens the ground subband states via an enhancement of the electron–electron scattering process. This process saturates in the high-field limit, however.

The inset of figure 5 shows the separate contributions due to scattering in and out for $\Omega_{12} = 10$ ps^{-1}. For a Fermi distribution at $T = 4$ K, Γ_1^{in} dominates for $k < k_f$, while Γ_1^{out} dominates for $k > k_f$. This is a direct result of the Pauli exclusion principle. For the case shown, however, this principle has less effect and both scattering terms contribute to the dephasing rate of a state in the ground subband. Such a state therefore becomes increasingly broad as the IR field intensifies. This process, however, depends very much on the density of electrons in the subband. At saturation, the electron density in the ground subband drops to half of its value in the uncoupled case, and the broadening reaches its maximum.

Now we consider the effect of detuning the infrared field on the intersubband transition and the electron–electron scattering process. We use the same structure as in figure 4, but with $\Delta_k = 10$ ps^{-1}. As shown in figure 4(b) and (d), the principal effect of detuning is the expected reduction of the transition rates. For similar Ω_{12} a smaller change in ρ_{11} and ρ_{22} is seen than for resonant coupling. There exists a distinct feature which was not expected, however. In figure 4(b) we see that, in contrast to figure 4(a), when $\Omega_{12} = 2$ and 5 ps^{-1} the distribution is less depleted near the Fermi edge than away from it. Therefore, in

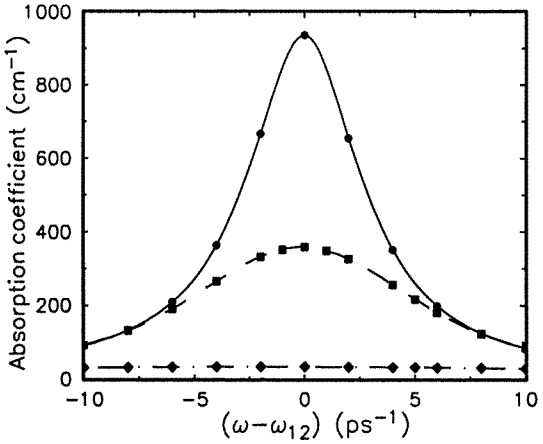

Figure 6. Absorption coefficient for $\Omega_{12} = 0.1$ ps^{-1} (circles), $\Omega_{12} = 2$ ps^{-1} (squares), and $\Omega_{12} = 10$ ps^{-1} (diamonds). ω_{12} is the frequency corresponding to the intersubband energy spacing. All other specifications are the same as those in figure 1.

figure 4(d), the distribution has a shoulder close to k_f, rather than a peak as in figure 4(b). This can be understood by noting that when the energy spacings are similar, the detuning of a field has much more effect on transitions which are associated with smaller dephasing rates or narrower transition states. Therefore, in detuned coupling conditions, if the field intensity is low enough that the k dependence of $\gamma_{12}^{\mathrm{e-e}}$ is significant, the states close to k_f should show less excitation than those with $k \sim 0$.

5. Absorption coefficient

There is much interest in studying the absorption coefficients of QWs in the high-field regime, where the field intensity is high enough to excite large numbers of electrons into the second conduction subband. This has often been studied in the past using formalisms which are suited only for the linear response regime, i.e. those using the RTA [6–9]. In some cases electron–electron interaction effects such as vortex correction (exciton effect) were included [11, 13], but even in these cases the damping rate in (28) was taken to be constant.

In figure 6 we show the absorption coefficient one obtains for the system of figure 4 when the electron–electron scattering effect is included. We assume that $\mu_{12} = e \times 2$ nm, which means that $\Omega_{12} = 1$ ps^{-1} corresponds to an intensity $I = 0.06$ MW cm^{-2} (I scales as the square of the Rabi frequency). For the weak-field case with $I = 0.6$ kW cm^{-2} ($\Omega_{12} = 0.1$ ps^{-1}), a non-saturated response is observed (circles). When the field intensity increases to 0.24 MW cm^{-2} ($\Omega_{12} = 2$ ps^{-1}), the absorption coefficient shows a strong saturation (squares). Further increase in the field intensity to 6 MW cm^{-2} ($\Omega_{12} = 10$ ps^{-1}) causes complete saturation (diamonds). These results are consistent with those shown in figure 4. In contrast to previous investigations, there is no structure in the spectrum's peak. The perturbative approaches used in those investigations produced such structure since the third-order term in the susceptibility made a negative contribution to the absorption coefficient which become significant at high field intensity [7, 8]. In addition, the use of the relaxation time approximation makes the previous results questionable, at best.

6. Linear response of infrared-driven quantum wells, generation of tunable gain spectrum

In this section we study the linear response of the IR-driven QW discussed in the last section to a second infrared field with the same polarization but much lower intensity. This is similar to previous studies, which have been carried out on optically driven two-level atomic systems [26]. One significant observation in these studies was that these systems produce two kinds of gain: one due to inversion of the dressed states with no bare-state inversion (the so-called Raman or hyper-Raman gain), and another due to stimulated Rayleigh scattering. Lasing based on both types of gain has been successfully demonstrated in atomic systems [27].

We show that although the two-subband QW system discussed in this paper is different in many ways from these atomic systems, it can demonstrate qualitatively similar dynamics. What distinguishes this investigation, however, is that the Raman gain in QW systems can happen at a range of frequencies comparable to that of the intersubband transition. This makes it suitable for IR and far-infrared lasing. As we will show below, the gain frequency can be made less than half that of the driving field by increasing the field intensity and detuning it positively with respect to the intersubband transition. Frequencies above $\frac{3}{2}\omega$ can be obtained by using negative detuning.

Before examining the detuned behaviour, we consider the linear response of the IR-coupled QW when the driving field is resonant with the intersubband transition ($\Delta_k = 0$). Evaluation of (23) for the system studied in figure 4 gives the results shown in figure 7. One can see for $\Omega_{12} = 0.1$ ps^{-1} ($I = 0.6$ kW cm^{-2}), where the system is weakly driven by the IR field (solid line), the response to the probe has a Lorentzian spectrum. For $\Omega_{12} = 2$ ps^{-1} ($I = 0.24$ MW cm^{-2}), however, the linear response spectrum becomes strongly broadened (dashed line). When the field intensity is increased to $\Omega_{12} = 5$ ps^{-1} ($I = 1.5$ MW cm^{-2}) the absorption spectrum develops into a triplet (dotted line). Ultimately, as the inset shows, for $\Omega_{12} = 10$ ps^{-1} ($I = 6$ MW cm^{-2}) the absorption spectrum becomes partially negative with three distinct peaks. This spectrum is similar to the Mollow spectrum obtained in atomic systems [14].

The linear response of the system when the strong field is detuned by $\Delta_k = 30$ ps^{-1} is shown in figure 8 for various IR intensities. The spectrum contains three basic features for all intensities: a blue-shifted absorption peak, a dispersive feature at the frequency of the driving field (marked by an arrow), and a gain peak at a frequency lower than that of the driving field. Increasing the field intensity causes suppression of the absorption peak, and increases both its blue shift and the red shift of the gain peak. For $\Omega_{12} \simeq 40$ ps^{-1} the gain spectrum reaches its maximum at 120 ps^{-1} below the higher transition subband. Further increase in the field intensity causes shifting of the gain spectrum to still lower frequencies, with a gradual decrease in peak gain. The structure at the driving field frequency does not shift but diminishes in amplitude with increasing field intensity.

7. Discussion

In this paper we studied the mutual effects of the ground subband electron–electron scattering process and intersubband transitions on each other in n-doped QWs. We considered the low-field regime where the system basically shows its intrinsic response, including the effect of electron–electron scattering on the intersubband polarization dephasing rates. We also studied these effects in the nonlinear regime where the IR field excites a significant number of electrons into the higher subband. In the latter case, our calculations predict the generation of steady-state non-Fermi electron distributions in both coupled subbands. In the past, such

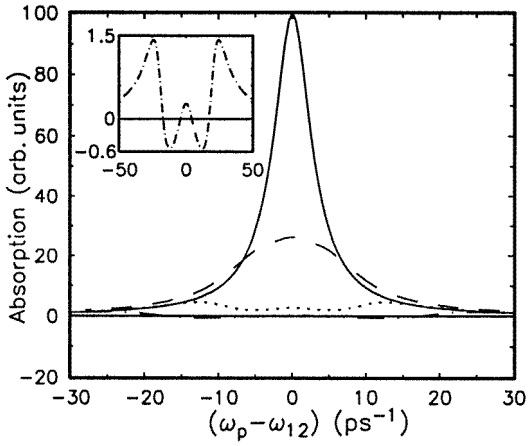

Figure 7. Linear absorption of the quantum well for various resonant infrared field intensities. Solid line corresponds to $\Omega_{12} = 0.1$ ps^{-1}, dashed line to $\Omega_{12} = 2$ ps^{-1}, dotted line to $\Omega_{12} = 5$ ps^{-1}, and dashed–dotted line to $\Omega_{12} = 10$ ps^{-1}. The inset shows $\Omega_{12} = 10$ ps^{-1} in more detail. Other specifications are the same as in figure 1.

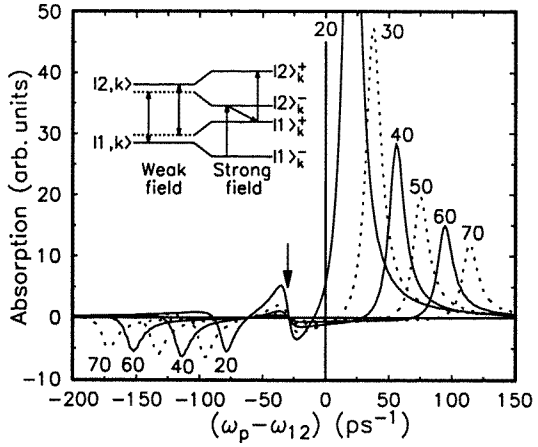

Figure 8. Linear absorption of the quantum well for various infrared field intensities with $\Delta = 30$ ps^{-1}. The numbers indicate the Rabi frequency of each curve, in ps^{-1}. The arrow shows the frequency of the pumping field. Other specifications are the same as in figure 4. Inset: the origin of the tunable gain peak. (See section 7.)

distributions have usually been studied only in transient cases, e.g. in studies of the evolution of photo-excited carriers generated by a fast interband or intersubband pulse using a probe field or photoluminescence measurement [28–30].

An important result was found in the case where the strongly driven system was probed by a weak IR field. Figures 7 and 8 showed generation of Mollow spectra in intersubband transitions in QWs. The results of figure 8, however, are particularly appealing for both practical and fundamental reasons. The dispersive feature seen in figure 8 is caused by competition between the gain and absorption processes [26]. In that respect, it is a quantum interference phenomenon. The gain in this feature is caused by stimulated Rayleigh

scattering. The tunable gain profile, however, is the result of absorption of two driving field photons and stimulated emission of one photon with the gain frequency, as indicated in the inset of figure 8. As the driving field intensity increases, the $|1\rangle_k^+$ and $|2\rangle_k^-$ dressed states move closer together in energy, and thus the gain frequency decreases. In atomic systems, this is usually called hyper-Raman or three-photon gain. Since this process transfers the system from the ground subband to a higher one, it is not gain without inversion. In fact, the dressed states are inverted, even though there is no inversion in the bare subbands [27].

The $GaAs/Ga_{0.7}Al_{0.3}As$ structure of figure 8 has an energy spacing between the conduction subbands of 144 meV [25]. A CO_2 laser with photon energy 124 meV then has a 20 meV detuning, close to that of figure 8. Considering a pulsed laser capable of producing intensities up to 200 MW cm^{-2} ($\Omega_{12} \simeq 60$ ps^{-1}), one sees that gain can be generated as much as 100 meV (150 ps^{-1}) below the higher subband energy. In other words, based on figure 8 the photon energy of the gain is continuously tunable between 44 meV and about 90 meV, simply by varying the intensity of the driving laser. This portion of the IR spectrum is currently underdeveloped in QWs [31], because the fast LO phonon scattering process foils the conventional inversion schemes for intersubband-based far-infrared lasers.

If the sign of the detuning were changed (i.e. $\Delta_k = -20$ meV), the absorption spectrum would be a mirror image of that in figure 8. The photon energy of the gain emission would then be 244 meV for a driving field with 164 meV photon energy and intensity of the order of 200 MW cm^{-2}. Using other QW structures, gain may be generated in other portions of the far-infrared spectrum.

Regarding figures 7 and 8, one should note that in contrast to an atomic system, where the spectrum contains a single transition line, in the case of a QW it is a superposition of a large number of transition lines with different damping rates (see (23)). These lines, which correspond to various values of k, have different linear spectra in general, but add up to give a single spectrum due to the nearly equal effective masses of the electrons.

The structure we chose was quite narrow (6.5 nm). This was crucial since the conduction band supported only two bound subbands and no quasi-bound subband [25]. This is not the case for wider QWs such as $GaAs/Ga_{0.7}Al_{0.3}As$ with 8.5 nm well width, which is usually considered in discussions of the IR coupling of QWs [32]. In this case, the quasi-bound subband is very close to the band edge, therefore its coupling to the two bound subbands has to be considered in the strong-field regime [33]. This subject is addressed in another paper [34].

The results of this paper can be tested experimentally using a conventional waveguide geometry [35]. Such a structure allows the strong IR and probe fields to enter the QW such that their electric fields have large components along the well's growth direction.

8. Conclusion

In this paper, we studied how the dephasing rates associated with intersubband transitions in n-doped QWs depend on the electron–electron scattering process for various IR intensities. We showed that, in contrast to previous investigations in which these rates were considered to be constant, they play a dynamic role in the response of the QW to IR fields polarized along its growth direction. By inspecting the electron distributions in both subbands, the k dependence of the dephasing rates was found to be important at low field intensities. As the intensity of the IR field increased, the k dependence became weaker but the magnitude of the dephasing rates increased significantly due to enhancement of the electron–electron scattering process in the ground subband. We also studied the linear response of the IR-driven quantum well to a weak field. The results showed generation of a gain spectrum

with large tunability. Various aspects of this process and its impact in intersubband-based IR and far-infrared QW lasers were discussed.

Acknowledgment

This research is supported by the Natural Sciences and Engineering Research Council of Canada.

References

[1] Kastalsky A 1993 *IEEE J. Quantum Electron.* **QE-29** 1112
[2] Levine B F, Gunapala S D and Kopt R F 1991 *Appl. Phys. Lett.* **58** 1551
[3] Hunsche S, Leo K, Kurz H and Kohler K 1994 *Phys. Rev.* B **50** 5791
[4] Faist J, Capasso F, Sirtori C, Sivco D, Hutchinson A, Chu S and Cho A 1993 *Appl. Phys. Lett.* **63** 1354
[5] Sadeghi S M and Meyer J 1996 *Phys. Rev.* B **53** 10 094
[6] Noda S, Uemura T, Yamashita T and Sasaki A 1992 *IEEE J. Quantum Electron.* **QE-28** 493
[7] Ahn D and Chuang S L 1987 *J. Appl. Phys.* **62** 3052
Ahn D and Chuang S L 1987 *IEEE J. Quantum Electron.* **QE-23** 2196
[8] Shao-hua and Feng Si-min 1991 *Phys. Rev.* B **44** 8165
[9] Roan E J and Chuang S L 1991 *J. Appl. Phys.* **69** 3249
[10] Sengers A J, Tsang L and Kuhn K J 1993 *Phys. Rev.* B **48** 15 116
[11] Huang D, Gumbs G and Manasreh M O 1995 *Phys. Rev.* B **52** 14 126
[12] Chang Yia-Chung and James R B 1989 *Phys. Rev.* B **39** 12 672
[13] Chuang S L, Luo M S C, Schmitt-Rink S and Pinczuk A 1992 *Phys. Rev.* B **46** 1897
[14] Mollow B R 1972 *Phys. Rev.* A **5** 2217
[15] Rossi F, Haas S and Kuhn T 1994 *Phys. Rev. Lett.* **72** 152
[16] Hughes S, Knorr A, Koch S W, Binder R, Indik R and Moloney J V 1996 *Solid State Commun.* **100** 555
[17] Binder R, Scott D, Paul A E, Lindberg M, Henneberger K and Koch S W 1992 *Phys. Rev.* B **45** 1107
[18] Smet J H, Fonstad C G and Hu Q 1996 *J. Appl. Phys.* **79** 9305
[19] Esipov S E and Levinson Y B 1987 *Adv. Phys.* **36** 331
[20] Schmitt-Rink S, Chemla D S and Haug H 1988 *Phys. Rev.* B **37** 941
[21] Bloss W L 1989 *J. Appl. Phys.* **66** 3639
[22] The shifts in the absorption spectrum due to the depolarization and exchange effects are partially compensated by the excitonic correlations (see [13]). In practice, one can consider $E^c(2,k) - E^c(1,k)$ in (22) to be the result of calculations of a QW structure in the weak-field regime including all these effects (see [21]). In the strong-field regime, the electron population remains confined to the well and the coupled subbands are extensively broadened. As a result, dynamic renormalization of the energy separation does not have a significant effect on the results of this paper.
[23] Asai H and Kawamura Y 1991 *Phys. Rev.* B **43** 4748
[24] Lyo S K 1991 *Phys. Rev.* B **43** 7091
[25] Bastard G, Brum J A and Ferreira R 1991 *Solid State Phys.* **44** 229
[26] Wu F Y, Ezebiel S, Ducloy M and Mollow B R 1977 *Phys. Rev. Lett.* **38** 1077
Grynberg G and Cohen-Tannoudji C 1993 *Opt. Commun.* **96** 150
[27] Lezama A, Zhu Yifu, Kanshar M and Mossberg T W 1990 *Phys. Rev.* B **41** 1576
Grandclement D, Grynberg G and Pinard M 1987 *Phys. Rev. Lett.* **59** 40
[28] Bohne G, Sure T, Ulbrich R G and Schafer W 1990 *Phys. Rev.* B **41** 7549
[29] Elsaesser T, Shah J, Rota L and Lugli P 1991 *Phys. Rev. Lett.* **66** 1757
[30] Lutgen S, Kaindl R A, Woerner M, Elsaesser T, Hase A and Kunzel H 1996 *Phys. Rev.* B **54** R17 343
[31] Sun G and Khurgin J B 1993 *IEEE J. Quantum Electron.* **QE-29** 1104
[32] Frohlich D, Neumann Ch, Spitzer S, Uebbing B and Zimmermann R 1991 *Proc. Int. Meeting on Optics of Excitons in Confined Systems (Giardini Naxos, 1991)* pp 227–36
[33] To see this effect on the interband excitonic response of an IR-coupled QW see Sadeghi S M, Young J F and Meyer J 1997 *Phys. Rev.* B **56** R15557
[34] Sadeghi S M, Leffler S R and Meyer J 1998 *Opt. Commun.* at press
[35] Ramsteiner M, Ralston J D, Koidl P, Dischler B, Biebl H, Wagner J and Ennen H 1990 *J. Appl. Phys.* **67** 3900